Available online at www.sciencedirect.com

ScienceDirect

Journal of the Franklin Institute 353 (2016) 1654–1671

Journal *of* The Franklin Institute

www.elsevier.com/locate/jfranklin

A Wavelet OFDM receiver for baseband power line communications

Fernando Cruz-Roldán[a,*], Freddy A. Pinto-Benel[a], José D. Osés del Campo[b], Manuel Blanco-Velasco[a]

[a]*Department of Teoría de la Señal y Comunicaciones, Escuela Politécnica Superior, Universidad de Alcalá, 28871 Alcalá de Henares, Spain*

[b]*Department of Teoría de la Señal y Comunicaciones, Escuela Técnica Superior de Ingeniería y Sistemas de Telecomunicación, Universidad Politécnica de Madrid, 28031 Madrid, Spain*

Received 6 February 2016; accepted 22 February 2016
Available online 2 March 2016

Abstract

Wavelet OFDM is one of the medium access techniques adopted by the IEEE P1901 working group for broadband power line communications (PLC). This paper reviews important aspects of baseband physical layer for broadband PLC, such as the scheme of modulation to obtain the transmitter and the characteristics of the recommended prototype filters. It further proposes a viable receiver system compatible with the transmitter and that provides perfect reconstruction characteristics in ideal environments. Furthermore, a procedure to perform the per-subcarrier frequency domain equalization, essential to deal with the power line channel effects at the receiver side, is also addressed. In order to greatly simplify the equalizer design, an efficient fast algorithm with reduced computational complexity is presented. Finally, this study is completed with several computer simulations, considering in-home PLC scenarios, to demonstrate the benefits of the proposed transceiver system.

*Corresponding author.
E-mail addresses: fernando.cruz@uah.es (F. Cruz-Roldán), freddy.pinto@uah.es (F.A. Pinto-Benel), david.oses@upm.es (J.D. Osés del Campo), manuel.blanco@uah.es (M. Blanco-Velasco).

http://dx.doi.org/10.1016/j.jfranklin.2016.02.015

1. Introduction

Discrete multitone (DMT) modulation, orthogonal frequency division multiplexing (OFDM), and filter bank multicarrier (FBMC) are channel partitioning methods that divide a transmission channel to form a set of parallel and ideally independent subchannels. DMT and OFDM are playing an important role in broadband digital wired and wireless communications [1,2] because they are easy to implement, achieve very high bandwidth efficiency, and lead to simple frequency domain equalizers to counteract multipath distortion. However, FBMC offers greater spectral separation in the information transmitted over each subcarrier, thus reducing the adjacent subchannel interference, showing higher robustness in noisy environments, and allowing for higher data throughput since the use of redundant data as the cyclic prefix (CP) can be avoided. A tutorial review of FBMC techniques and comparisons with DFT-based transceivers in various applications can be found in [3–6].

FBMC is not only a promising candidate for 5th generation (5G) systems [3,4], but also a medium access technique already recommended for high-speed communications via electric power lines [7,8]. Communication networks will play a crucial role in the development of smart grid which aim to not only making electricity delivery more reliable, economical and sustainable, but also the convergence of information and communication technologies with power system engineering. For the above reasons, this field is subject of many research efforts to propose innovative solutions and new applications (see, e.g., [9,10]).

The standard proposed by the IEEE P1901 working group has promoted windowed OFDM and FBMC (Wavelet OFDM) as medium access techniques for power line communications (PLC) [11]. Originally, filter bank system in a synthesis-analysis configuration was denoted transmultiplexer (TMUX) [12,13], although the terminology adopted in [11] to denote the TMUX has been Wavelet OFDM. However, the above denomination is a misnomer [14] because, as we will show later, the recommended Wavelet OFDM is based on cosine modulated (CM) filter banks, and there exists another class of multicarrier systems that are based on true wavelets (e.g., [15]).

The contribution of this paper is threefold. First, the understanding on the Wavelet OFDM for baseband high-speed communications over power line networks is extended. Some key features, as the kind of FBMC proposed as transmitter, or the waveforms recommended as prototype filters to obtain the transmitting filters, are clarified. Also as novel contribution, a set of expressions to obtain the coefficients of these prototype filters given in [11] is presented. Second, efficient structures for both transmitter and receiver, based on polyphase filters [16], are also proposed. The coefficients of the polyphase filters are obtained from the prototype filter, and each pair of filters can be implemented using a direct or a transpose form, or lattice structures, singly or in pairs. The computational complexities of the proposed fast algorithms of implementation, for each different structure of polyphase filters, are also derived. Third, we finally propose and investigate the performance of an easy frequency-domain equalizer system, which can help to correct the distortion of the power line channel.

The rest of this paper is organized as follows. In Section 2, we address the modulation scheme of the transmitter and we present several expressions to obtain the prototype filters from which the transmitting and the receiving subchannels filters are constructed. Section 3 presents our proposal of receiver and the way of implementing it. Section 4 describes a simple frequency-domain channel equalizer to compensate for the transmission channel effects. Section 5 provides the performance evaluation of the Wavelet OFDM transceiver in a PLC scenario, and finally, concluding remarks are given in Section 6.

Notation. Bold-typed letters indicate vectors (lower case) and matrices (upper case). Notation $\mathbf{A}^T$ represents the transpose of $\mathbf{A}$. Matrix $\mathbf{I}$ denotes the identity matrix, and $\mathbf{J}$ denotes the counter-identity matrix:

$$\mathbf{J} = \begin{pmatrix} 0 & \cdots & 0 & 1 \\ 0 & \cdots & 1 & 0 \\ \vdots & & \vdots & \vdots \\ 1 & \cdots & 0 & 0 \end{pmatrix}.$$

$\mathbf{\Gamma}$ is an $M \times M$ diagonal matrix with elements $[\mathbf{\Gamma}]_{k,k} = (-1)^k$, for $0 \le k \le (M-1)$. The delay chain $\mathbf{t}(z)$ is the column vector

$$\mathbf{t}(z) = \begin{bmatrix} 1 & z^{-1} & \cdots & z^{-(M-1)} \end{bmatrix}^T.$$

2. Modulated filter bank multicarrier system recommended for PLC

Modulated FBMC systems are designed applying a trigonometric or exponential modulation to one or two prototype filters (see, e.g., [17,18] and the references therein). In this way, the design of the prototype filter is a key point in order to get an FBMC with either perfect or nearly perfect reconstruction (PR or NPR) property. In this section, we describe the filter bank multicarrier transmitter and the prototype filters that are proposed as medium access technique in the baseband Wavelet OFDM physical layer [11].

2.1. Transmitter

The standard considers three different number of subchannels: $M=512$, 1024, 2048, and the following prototype filter lengths: $N = 2$ mM, with $m=2$ or $m=3$. On the other hand, the corresponding frame may be transmitted either baseband or by modulation to a bandpass carrier [11]. We focus for the rest of this work on $M=512$ subchannels and baseband, mandatory for in-home and access applications.

In this case, the equation to obtain the time-domain waveform signal for the frame body is stated as follows [11, p. 1194]:

$$\frac{1}{16}\left[\sum_{k=0}^{3}\sum_{\substack{c=0 \\ \mathbb{K}_{on}}}^{N_{used}-1} p[n+512k]\cdot \cos\left(\frac{\pi}{512}\cdot\left((n+512k)+\frac{512+1}{2}\right)\left(c+\frac{1}{2}\right)+\theta_k\right)\right], \tag{1}$$

where an overlap factor of 4 is assumed ($m=2$), $0 \le n < 512$, $\mathbb{K}_{on} \subseteq \{0,\ldots,511\}$ is the set of active subchannels defined by the tone mask [11], N_{used} denotes the number of used carriers (512 in this case), $p[n]$ is the prototype filter, and θ_k is a phase vector for peak power reduction. The values of θ_k for $M=512$ are defined in [11, Tables 14–10], and they equal 0 or π. When the total number of used carriers exceeds 512, the phase vector is constituted by repeating the phase group from carrier number 1–512.

It is important to note that Eq. (1) can be rewritten as:

$$\frac{1}{16}\sum_{\substack{c=0\\ \mathbb{K}_{on}}}^{511} p[n]\cdot \cos\left(\frac{\pi}{512}\left(n+\frac{512+1}{2}\right)\left(c+\frac{1}{2}\right)+\theta_k\right), \tag{2}$$

for $0\le n\le 2047$. Notice that in Eq. (2) the scale factor $\frac{1}{16}$ matches with $\sqrt{\frac{2}{M}}$, and that the phase vector θ_k only affects the sign of the time-domain waveform, since it equals 0 or π. Accordingly, the impulse-response coefficients of the M-channel transmitting filters are given by

$$f_k[n]=\sqrt{\frac{2}{M}}\cdot p[n]\cdot \cos\left[\left(k+\frac{1}{2}\right)\frac{\pi}{M}\left(n+\frac{M+1}{2}\right)\right]\cdot \cos(\theta_k), \tag{3}$$

where $k\in\mathbb{K}_{on}$. This expression, excluding the term $\cos(\theta_k)$, is nothing but the synthesis filters of an extended lapped transform (ELT) introduced by Malvar [19].

2.2. Prototype filters

Different prototype filters are proposed in the standard for the cases of $M=512$, 1024 and 2048 subchannels, and for overlapping factors m equals 2 or 3. For the case of $m=2$, the prototype filter coefficients $p[n]$ can be obtained from a "mother filter" $h[n]$, given in [11, p. 1205], as follows:

- $M=512$ subchannels:
$$p[n]=\tfrac{1}{2}\{h[4n+1]+h[4n+2]\}\quad 0\le n<2M.$$
- $M=1024$ subchannels:
$$p[n]=\tfrac{1}{2}\{h[2n]+h[2n+1]\}\quad 0\le n<2M.$$
- $M=2048$ subchannels:
$$p[n]=h[n]\quad 0\le n<2M.$$
- For $M=512, 1024, 2048$ subchannels:
$$p[n]=p[4M-1-n]\quad 2M\le n<4M.$$

It can be seen that the resulting prototype filter presents an even symmetry ($p[N-1-n]=p[n]$). Unfortunately, the standard does not provide expressions that allow designers to quickly obtain the corresponding coefficients. In this sense, we have noticed that this prototype filter belongs to a family of windows proposed by Malvar [19] which fulfills the perfect reconstruction (PR) property in the context of filter bank. Specifically, let us consider the following angles:

$$\vartheta_{i0}=-\frac{\pi}{2}+\mu_{i+M/2},\quad \vartheta_{i1}=-\frac{\pi}{2}+\mu_{M/2-1-i},$$

where

$$\mu_i=\left[\left(\frac{0.7}{2M}\right)(2i+1)+0.3\right]\frac{(2i+1)\pi}{8M},$$

for $0\le i\le(M-1)$. The prototype filter coefficients in [11, p. 1205], for $M=512$ and $m=2$, can be easily obtained as follows:

$$p[n]=\cos(\vartheta_{n0})\cdot\cos(\vartheta_{n1}),$$

$$p[M-1-n] = \sin(\vartheta_{n0}) \cdot \cos(\vartheta_{n1}),$$
$$p[M+n] = \cos(\vartheta_{n0}) \cdot \sin(\vartheta_{n1}),$$
$$p[2M-1-n] = -\sin(\vartheta_{n0}) \cdot \sin(\vartheta_{n1}),$$

for $0 \le n \le (M/2-1)$.

3. Proposed transceiver implementation

An additional appealing feature of ELT is that very fast algorithms, which depend on the prototype filter length $N = 2$ mM, can be used to efficiently perform it. The goal of this section is to connect the theory of efficient ELT implementation with Wavelet OFDM, showing different building blocks to carry out the PLC transceiver.

3.1. Transmitting bank implementation with polyphase filters

The aim of this subsection is to present an implementation of the wavelet transceiver using polyphase filters at the transmitting filter bank. To this goal, let us formulate Eq. (3) in the z-domain using matrices. Let $P(z) = \sum_{n=0}^{N-1} p[n] \cdot z^{-n}$ be the $(N-1)$th-order prototype filter transfer function, which can be expressed by means of the $2M$ type-I polyphase decomposition [16]:

$$P(z) = \sum_{\ell=0}^{2M-1} z^{-\ell} G_\ell\left(z^{2M}\right),$$

where $G_\ell\left(z^{2M}\right)$ is the z-transform of $g_\ell[n] = p[2nM + \ell]$, $\ell = 0, \ldots, (2M-1)$. From the above equation, the transmitting filters $F_k(z)$ can be expressed in the following way:

$$\begin{aligned} F_k(z) &= \sum_{n=0}^{N-1} f_k[n] z^{-n} \\ &= \sum_{\ell=0}^{2M-1} c_{\ell,k}^{(f)} \cdot \cos\,\theta_k \cdot z^{-\ell} \cdot G_\ell\left(-z^{2M}\right), \end{aligned} \tag{4}$$

where

$$c_{\ell,k}^{(f)} = \sqrt{\frac{2}{M}} \cdot \cos\left(\left(k+\frac{1}{2}\right)\frac{\pi}{M} \cdot \left(\ell + \frac{M+1}{2}\right)\right), \tag{5}$$

for $0 \le k \le (M-1)$. The above relation is the result of the periodicity of the cosine function which satisfies [20]:

$$c_{\ell+2mM,k}^{(f)} = (-1)^m c_{\ell,k}^{(f)}.$$

The transmitting filters of Eq. (4) are written in a matrix form as:

$$\begin{aligned} \mathbf{f}^T(z) &= \begin{bmatrix} F_0(z) & F_1(z) & \cdots & F_{M-1}(z) \end{bmatrix} \\ &= \mathbf{t}^T(z) \cdot \begin{bmatrix} \mathbf{g}_0\left(z^{2M}\right) & z^{-M}\mathbf{g}_1\left(z^{2M}\right) \end{bmatrix} \cdot \hat{\mathbf{C}}_{Tx}, \end{aligned}$$

where

$$\left[\hat{\mathbf{C}}_{Tx}\right]_{\ell,k} = c_{\ell,k}^{(f)} \cdot \cos\,\theta_k,$$

and $\mathbf{g}_0$ and $\mathbf{g}_1$ are $M \times M$ diagonal matrices with elements

$$\left[\mathbf{g}_0(z)\right]_{k,k} = G_k(-z),$$
$$\left[\mathbf{g}_1(z)\right]_{k,k} = G_{k+M}(-z).$$

Let us partition $\hat{\mathbf{C}}_{Tx}$ as

$$\hat{\mathbf{C}}_{Tx} = \begin{bmatrix} \mathbf{B}_0 \\ \mathbf{B}_1 \end{bmatrix} \cdot \mathbf{\Theta},$$

$\mathbf{\Theta}$ is an $M \times M$ diagonal matrix with elements $[\mathbf{\Theta}]_{k,k} = \cos(\theta_k)$, $\mathbf{B}_0$ and $\mathbf{B}_1$ are also $M \times M$ matrices, being the elements of the first one given by

$$[\mathbf{B}_0]_{\ell,k} = c_{\ell,k}^{(4e)} \cdot \cos(\lambda_{k0}) + s_{\ell,k}^{(4e)} \cdot \sin(\lambda_{k0}),$$

with

$$[\mathbf{C}_{4e}]_{\ell,k} = c_{\ell,k}^{(4e)} = \sqrt{\frac{2}{M}} \cos\left(\left(k+\frac{1}{2}\right)\frac{\pi}{M} \cdot \left(\ell+\frac{1}{2}\right)\right),$$
$$[\mathbf{S}_{4e}]_{\ell,k} = s_{\ell,k}^{(4e)} = \sqrt{\frac{2}{M}} \sin\left(\left(k+\frac{1}{2}\right)\frac{\pi}{M} \cdot \left(\ell+\frac{1}{2}\right)\right),$$
$$[\mathbf{\Lambda}_{C0}]_{k,k} = \cos(\lambda_{k0}) = \cos\left(\left(k+\frac{1}{2}\right)\frac{\pi}{2}\right),$$
$$[\mathbf{\Lambda}_{S0}]_{k,k} = \sin(\lambda_{k0}) = \sin\left(\left(k+\frac{1}{2}\right)\frac{\pi}{2}\right).$$

Notice that $\mathbf{C}_{4e}$ and $\mathbf{S}_{4e}$ are, respectively, the type-IV even discrete cosine transform (DCT4e) and the type-IV even discrete sine transform (DST4e) matrices [21,22].

Regarding the second matrix $\mathbf{B}_1$, each of its elements can be expressed as

$$[\mathbf{B}_1]_{\ell,k} = c_{\ell,k}^{(4e)} \cdot \cos(\lambda_{k1}) + s_{\ell,k}^{(4e)} \cdot \sin(\lambda_{k1}),$$

where

$$[\mathbf{\Lambda}_{C1}]_{k,k} = \cos(\lambda_{k1}) = \cos\left(\left(k+\frac{1}{2}\right)\frac{3\pi}{2}\right),$$
$$[\mathbf{\Lambda}_{S1}]_{k,k} = \sin(\lambda_{k1}) = \sin\left(\left(k+\frac{1}{2}\right)\frac{3\pi}{2}\right).$$

Thus, matrices $\mathbf{B}_0$ and $\mathbf{B}_1$ can be written as given below:

$$\mathbf{B}_0 = \mathbf{C}_{4e} \cdot \mathbf{\Lambda}_{C0} - \mathbf{S}_{4e} \cdot \mathbf{\Lambda}_{S0}, \tag{6a}$$

$$\mathbf{B}_1 = \mathbf{C}_{4e} \cdot \mathbf{\Lambda}_{C1} - \mathbf{S}_{4e} \cdot \mathbf{\Lambda}_{S1}. \tag{6b}$$

Important properties are $\mathbf{\Lambda}_{S0} = \mathbf{\Gamma} \cdot \mathbf{\Lambda}_{C0}$, $\mathbf{\Lambda}_{C1} = -\mathbf{\Lambda}_{C0}$, $\mathbf{\Lambda}_{S1} = \mathbf{\Gamma} \cdot \mathbf{\Lambda}_{C0}$, and $\mathbf{S}_{4e} \cdot \mathbf{\Gamma} = \mathbf{J} \cdot \mathbf{C}_{4e}$. Using the above, we have

$$\mathbf{B}_0 = (\mathbf{I} - \mathbf{J}) \cdot \mathbf{C}_{4e} \cdot \mathbf{\Lambda}_{C0}, \tag{7a}$$

$$\mathbf{B}_1 = (-\mathbf{I} - \mathbf{J}) \cdot \mathbf{C}_{4e} \cdot \mathbf{\Lambda}_{C0}. \tag{7b}$$

Finally, the transmitting filters can be expressed as follows:

$$\mathbf{f}^T(z) = \mathbf{t}^T(z) \cdot \left[\mathbf{g}_0\left(z^{2M}\right) \quad z^{-M}\mathbf{g}_1\left(z^{2M}\right) \right] \times \begin{bmatrix} (\mathbf{I}-\mathbf{J}) \\ (-\mathbf{I}-\mathbf{J}) \end{bmatrix} \cdot \mathbf{C}_{4e} \cdot \mathbf{\Lambda}_{C0} \cdot \mathbf{\Theta}.$$

3.2. Receiving bank implementation with polyphase filters

The transmitter given by Eq. (3) leads us to propose a receiver based on the scheme of modulation recommended by Malvar for the analysis bank or direct ELT [19]. In addition, the phase factors θ_k of Eq. (3) must be included to guarantee perfect symbol recovery in absence of a transmission channel and noise. This scheme of cosine modulation is

$$h_k[n] = \sqrt{\frac{2}{M}} \cdot p[n] \cdot \cos\left[\left(k+\frac{1}{2}\right)\frac{\pi}{M} \cdot \left(N-1-n+\frac{M+1}{2}\right)\right] \cdot \cos(\theta_k). \tag{8}$$

Taking the z transform in Eq. (8), we obtain the system function for the receiving filters $H_k(z)$:

$$H_k(z) = \sum_{n=0}^{N-1} h_k[n] z^{-n} = \sum_{\ell=0}^{2M-1} c_{k,\ell}^{(h} \cdot \cos\theta_k \cdot z^{-\ell} \cdot G_\ell\left(-z^{2M}\right), \tag{9}$$

where

$$c_{k,\ell}^{(h} = \sqrt{\frac{2}{M}} \cdot \cos\left(\left(k+\frac{1}{2}\right)\frac{\pi}{M} \cdot \left(N-1-\ell+\frac{M+1}{2}\right)\right).$$

Using matrices, the transmitting filters can be expressed as

$$\mathbf{h}(z) = \begin{bmatrix} H_0(z) \\ H_1(z) \\ \vdots \\ H_{M-1}(z) \end{bmatrix} = \hat{\mathbf{C}}_{Rx} \cdot \begin{bmatrix} \mathbf{g}_0\left(z^{2M}\right) \\ z^{-M}\mathbf{g}_1\left(z^{2M}\right) \end{bmatrix} \cdot \mathbf{t}(z),$$

with

$$\left[\hat{\mathbf{C}}_{Rx}\right]_{k,\ell} = c_{k,\ell}^{(h} \cdot \cos\theta_k.$$

Notice that now the fast implementation of the receiving system depends on the value of m. As we have mentioned, the standard recommends two different overlapping factors: $m=2$ and $m=3$. Operating as in the previous subsection, the following result is obtained:

$$\hat{\mathbf{C}}_{Rx} = \mathbf{\Theta} \cdot \mathbf{\Lambda}_{C0} \cdot \mathbf{C}_{4e} \cdot \left[\alpha(\mathbf{I}+\mathbf{J}) \quad \alpha(\mathbf{I}-\mathbf{J}) \right],$$

where $\alpha = 1$ for $m=2$, and $\alpha = -1$ for $m=3$. Therefore, the final expression that characterizes the proposed receiver is the following:

$$\mathbf{h}(z) = \mathbf{\Theta} \cdot \mathbf{\Lambda}_{C0} \cdot \mathbf{C}_{4e} \cdot \left[\alpha(\mathbf{I}+\mathbf{J}) \quad \alpha(\mathbf{I}-\mathbf{J}) \right] \cdot \begin{bmatrix} \mathbf{g}_0\left(z^{2M}\right) \\ z^{-M}\mathbf{g}_1\left(z^{2M}\right) \end{bmatrix} \mathbf{t}(z). \tag{10}$$

The implementation of the whole transceiver, including both the transmitting and the receiving stages, is depicted in Fig. 1. In this figure, the matrix $\mathbf{\Lambda}_{cn} = \sqrt{2} \cdot \mathbf{\Theta} \cdot \mathbf{\Lambda}_{C0}$, where

$$[\mathbf{\Lambda}_{C0}]_{k,k} = \cos(\lambda_{k0}) = \cos\left(\left(k+\frac{1}{2}\right)\frac{\pi}{2}\right).$$

This leads to $[\mathbf{\Lambda}_{cn}]_{k,k} = \pm 1$. To compensate for the constant $\sqrt{2}$, its inverse value is multiplying both the transmitting and the receiving signals.

3.3. Polyphase filters with lattice structures

In the implementation of Fig. 1, the output signals of the corresponding transmitting polyphase filters are added. On the receiving side, each pair of polyphase filters are fed with the same input signal. Note that Wavelet OFDM follows the modulation scheme given in Eq. (3) and, according to our proposal, the receiver is obtained using Eq. (8). The prototype filter proposed in the standard has linear-phase, and the same prototype is employed for both the transmitting and the receiving sides. Moreover, the type-I polyphase components of each filter recommended in [11]

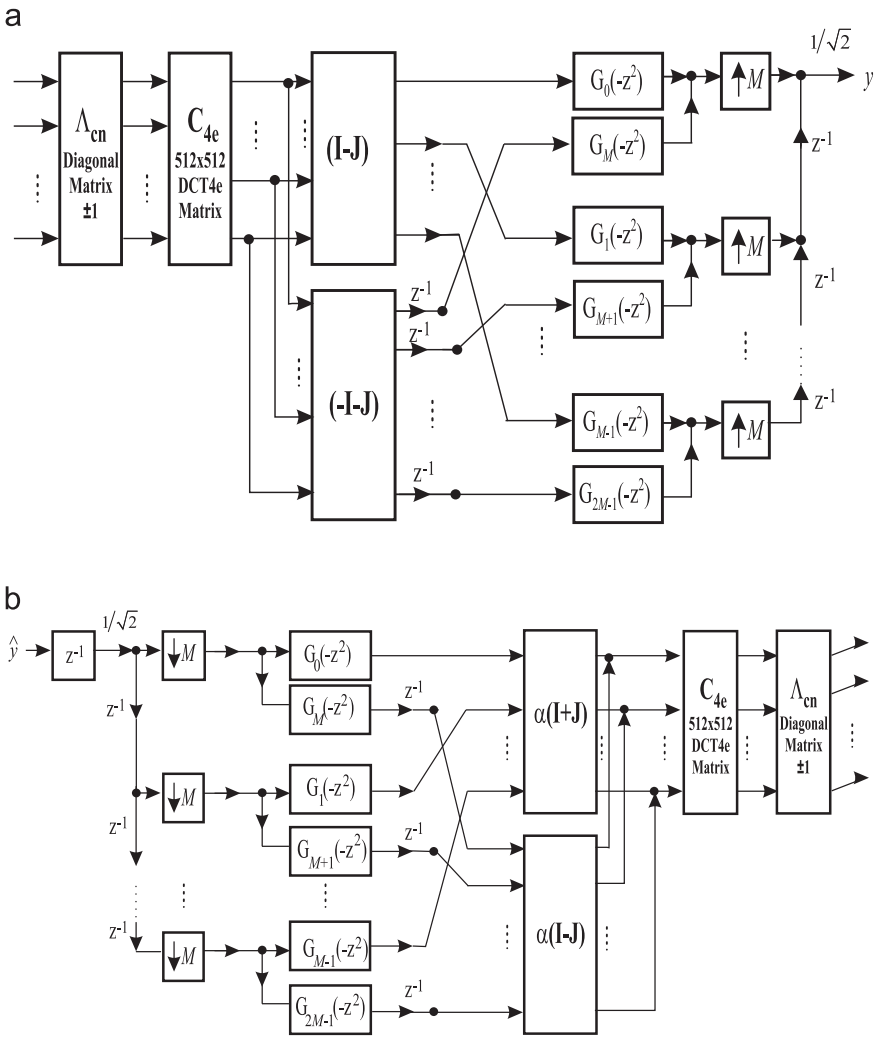

Fig. 1. Block diagram of the wavelet OFDM transceiver implemented with polyphase filters ($M=512$). (a) Transmitter. (b) Receiver.

satisfy

$$\tilde{G}_i(z)\cdot G_i(z)+\tilde{G}_{i+M}(z)\cdot G_{i+M}(z)=1,$$

where $\tilde{G}(z)=G^*\left(z^{-1}\right)$, which means that the filter bank is paraunitary. This leads to a joint implementation of pairs of filters, i.e., that each pair of polyphase filters can be implemented at a time via lattice structures [23].

Let us consider again the case of $N=2$ mM for $M=512$ and $m=2$. Each polyphase filter of Fig. 2(a) has a length equals $2m-1=3$, and the intermediate coefficient is zero. Therefore, the ith and $i+M$th polyphase filters can be expressed respectively as

$$G_i(-z^2)=a+bz^{-2},\quad G_{i+M}(-z^2)=c+dz^{-2}.$$

The lattice coefficients of the structure of Fig. 2(b) are obtained as [23]

$$v_{2n}=\frac{-d}{\sqrt{b^2+d^2}},\quad \hat{v}_{2n}=\frac{b}{\sqrt{b^2+d^2}},$$
$$r_{0n}=\frac{-ad+bc}{\sqrt{b^2+d^2}},\quad s_{0n}=-\sqrt{b^2+d^2}.$$

Each normalized lattice structure of Fig. 2(b) has six multipliers. As alternative, two equivalent denormalized lattices, which require four multipliers, can be obtained [23]. In the first denormalized structure depicted in Fig. 2(c), the coefficients are calculated as:

$$v_{2d}=\frac{\hat{v}_{2n}}{v_{2n}},\quad r_{0d}=r_{0n}\cdot v_{2n},\quad s_{0d}=s_{0n}\cdot v_{2n}.$$

Similarly, the coefficients of the second denormalized structure (Fig. 2(d)) are given by

$$v_{2a}=\frac{v_{2n}}{\hat{v}_{2n}},\quad r_{0a}=r_{0n}\cdot \hat{v}_{2n},\quad s_{0a}=s_{0n}\cdot \hat{v}_{2n}.$$

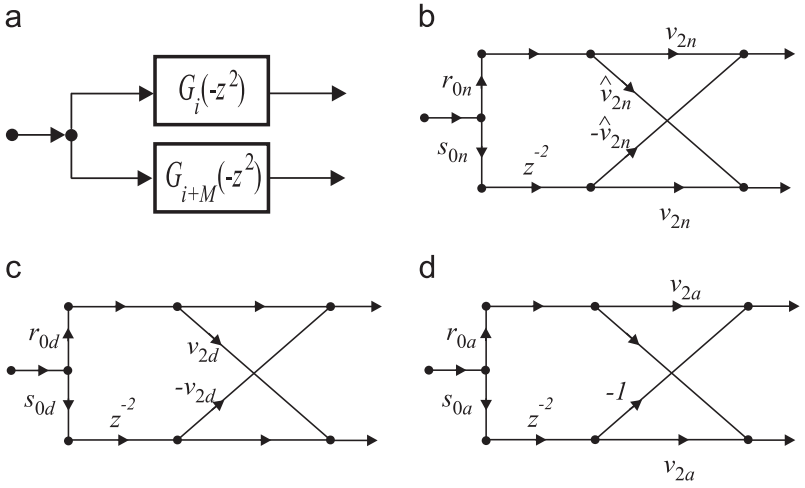

Fig. 2. (a) Pair of polyphase filters. (b) Implementation using normalized lattice structure. (c) Implementation using denormalized lattice structure requiring four multipliers. (d) Alternative implementation using denormalized lattice structure also requiring four multipliers.

3.4. Computational complexity

In this part, we discuss several algorithms of the proposed Wavelet OFDM receiver in terms of arithmetic complexity. Central to the operation of this system is DCT4e as the basic transform block at both the receiver and the transmitter sides. This transform has played a key role in numerous applications, such as audio signals compression, and thus many fast computational structures can be found (see, e.g., [24–26]). Tables 1 and 2 include the computational cost of some efficient algorithms, and as it can be seen, the algorithm proposed in [26] provides the lower flop count and the lower number of multiplications. Notice that exactly the same flop count is obtained for the DST4e, since it is related to DCT4e by means of sign changes and reversals of the input and output sequences [26].

Table 3 includes the computational complexity of the receiver of Fig. 3, counted for length-M blocks, and considering the three different implementations shown in Fig. 2 for each pair of polyphase filters. To obtain these results, sign changes have not been computed as multiplications, and DCT4e is implemented with the procedure presented in [26]. Moreover, MUL_{best} and ADD_{best} denote, respectively, the number of multiplications and additons necessary to carry out the algorithm in [26]. The remaining multiplications are contributed by the first

Table 1
Number of multiplications for various efficient implementations of DCT4e for length-M blocks.

Algorithm	**Multiplications (MUL)**
Ref. [24]	$\frac{M}{2}\left(\log_2 M+2\right)$
Ref. [25]	$M\log_2 M+\frac{2}{3}M-\frac{2}{3}(-1)^{\log_2 M}$
Ref. [26]	$MUL_{best}=\frac{5M}{9}\log_2 M+\frac{2}{9}(-1)^{\log_2 M}\log_2 M+\frac{10}{27}M-\frac{10}{27}(-1)^{\log_2 M}$

Table 2
Number of additions for various efficient implementations of DCT4e for length-M blocks.

Algorithm	**Additions (ADD)**
Ref. [24]	$\frac{3M}{2}\log_2 M$
Ref. [25]	$\frac{4M}{3}\log_2 M-\frac{2}{9}M+\frac{2}{9}(-1)^{\log_2 M}$
Ref. [26]	$ADD_{best}=\frac{4M}{3}\log_2 M+\frac{7}{9}M+\frac{2}{9}(-1)^{\log_2 M}$

Table 3
Computational complexity of the efficient polyphase receivers of Fig. 3 ($M=512$, $m=2$ and $N=2048$).

Implementation	MPIS	APIS
Direct or transpose	$7M+2\cdot MUL_{best}$	$9M+2\cdot ADD_{best}$
Normalized lattices	$9M+2\cdot MUL_{best}$	$9M+2\cdot ADD_{best}$
Denormalized lattices	$7M+2\cdot MUL_{best}$	$9M+2\cdot ADD_{best}$

constant term (M), the polyphase filtering ($4M$ direct or transpose form, $6M$ normalized and $4M$ denormalized lattices), and the 0-ASCET equalizers ($2M$). The additions are contributed by the polyphase filtering ($2M$), the operations with matrices $\mathbf{I}$ and $\mathbf{J}$ ($4M$), their outputs ($2M$) and the 0-ASCETs outputs (M). Although the computational complexity is almost the same for the three systems, the most suitable fast algorithms are based on direct/transpose filters or denormalized lattices.

4. Frequency domain equalization

One of the main drawbacks of the FBMC systems is the channel equalization process, which is not as understandable and efficient as for the standardized DFT-based multicarrier modulation (MCM). In [27], one of the simplest equalizer to correct the channel effects for CM FBMC systems is proposed. It is referred to as adaptive sine-modulated/cosine-modulated filter bank equalizer for transmultiplexer (ASCET). From the analysis (receiving) stage of a CM FBMC system, the ASCET compensates for the channel distortion using an analysis sine modulated (SM) FBMC system connected in parallel to the former. In addition, a frequency domain equalizer (FEQ) is included at each receiving cosine and sine modulated filter banks.

The use of ASCET for PLC is proposed in [28], but not for the ELT-based FBMC system proposed in the Wavelet OFDM physical layer. In this section, we derive an appropriate scheme that can be used for the transmitter recommended in [11].

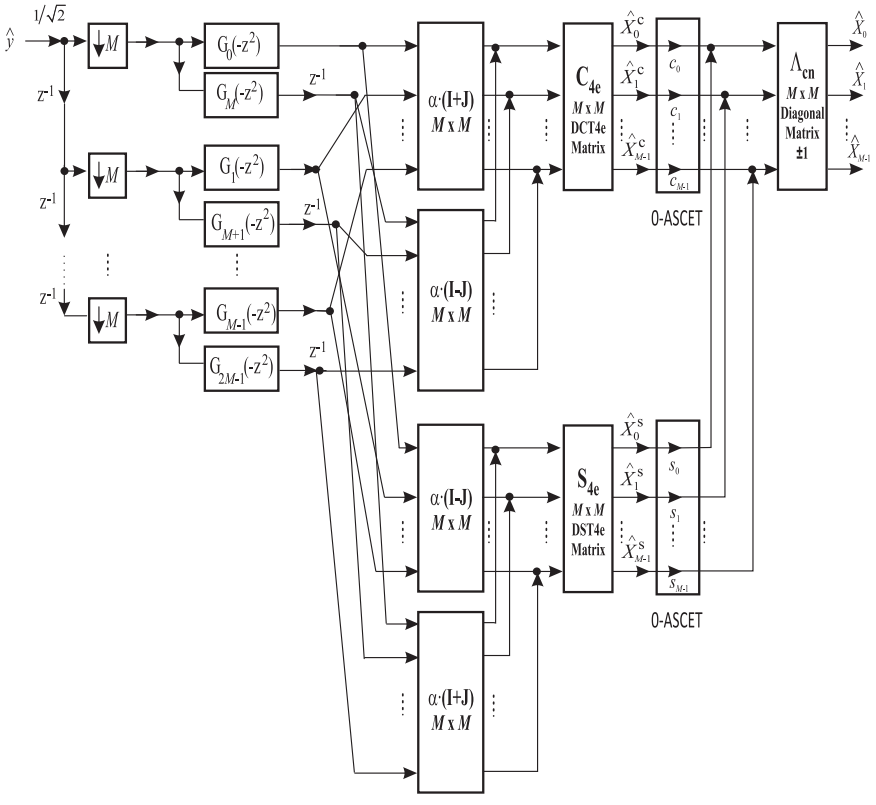

Fig. 3. Fast implementation of the Wavelet OFDM receiver including a 0-ASCET with polyphase filters.

4.1. Proposed SM FBMC and efficient implementation

We proposed as SM FBMC for the ASCET the analysis stage of an ELT-based sine-modulated filter bank (SMFB), in which the impulse responses of the analysis filters are given by

$$h_k^{(s}[n] = \sqrt{\frac{2}{M}} \cdot p[n] \cdot \sin\left[\left(k+\frac{1}{2}\right)\frac{\pi}{M}\cdot\left(N-1-n+\frac{M+1}{2}\right)\right] \cdot \cos(\theta_k). \tag{11}$$

To proceed with the matrix formulation for the sine-modulated analysis filter bank with polyphase filters, we consider the system function $H_k^s(z)$ of each filter of Eq. (11):

$$H_k^{(s}(z) = \sum_{n=0}^{N-1} h_k^{(s}[n] z^{-n} = \sum_{\ell=0}^{2M-1} s_{k,\ell}^{(h} \cdot \cos\theta_k \cdot z^{-\ell} \cdot G_\ell\left(-z^{2M}\right), \tag{12}$$

for $0 \le k \le (M-1)$, and

$$s_{k,\ell}^{(h} = \sqrt{\frac{2}{M}} \cdot \sin\left(\left(k+\frac{1}{2}\right)\frac{\pi}{M}\cdot\left(N-1-\ell+\frac{M+1}{2}\right)\right).$$

Operating as previously, a compact expression for the analysis SMFB is derived:

$$\mathbf{h}^{(s}(z) = \boldsymbol{\Theta}\cdot\boldsymbol{\Lambda}_{C0}\cdot\mathbf{S}_{4e}\cdot\begin{bmatrix}\alpha(\mathbf{J}-\mathbf{I}) & \alpha(\mathbf{J}+\mathbf{I})\end{bmatrix}\cdot\begin{bmatrix}\mathbf{g}_0\left(z^{2M}\right)\\ z^{-M}\mathbf{g}_1\left(z^{2M}\right)\end{bmatrix}\mathbf{t}(z). \tag{13}$$

4.2. FEQ coefficients

Once the SMFB is defined, we focus now on the equalizer block $E(z)$, which is included at each output of both the CMFB and the SMFB receiving system. Following the minimum mean square error (MMSE) criterion and under additive white Gaussian noise (AWGN), the kth subchannel equalizer block is defined as follows:

$$E_k(\Omega) = \frac{H_{ch}^*(\Omega)}{\left|H_{ch}(\Omega)\right|^2 + \dfrac{1}{SNR}}, \tag{14}$$

where $H_{ch}(\Omega)$ is the channel frequency response and SNR is the signal-to-noise ratio.

4.2.1. 0–ASCET

The complex function $E_k(\Omega)$ can be expressed as

$$E_k(\Omega)\Big|_{\Omega=(2k+1)\frac{2\pi}{4M}} = c_k - j\cdot s_k,$$

for $0 \le k < M$, where c_k and s_k are the real and the imaginary parts of E_k, respectively. In the zero-order ASCET (0-ASCET), the transmission channel effects are compensated for by multiplying each output of the CM and SM receiving filter bank by the constant numbers c_k and s_k, respectively.

Fig. 3 depicts the efficient implementation of the whole receiver system, including the 0-ASCET stages, with polyphase filters. The ASCET is composed by the CM analysis filters given

in Eq. (8), and by the SM analysis filters described by Eq. (11). Notice that there are some common terms in these expressions that can be grouped in order to implement them simultaneously and, therefore, to reduce the number of operations.

4.2.2. 1-ASCET

As it is claimed in [27] that the 0-ASCET is adequate for channels with no fast variations within the subchannel bandwidth. Unfortunately, this is not the case of the PLC channel and, therefore, it is necessary to design other kinds of equalizers that improve the system performance. These equalizers are called *L*-order (*L*-) ASCET. Fig. 4 depicts the block diagram of the 1-ASCET.

Following the development presented in [29], a 3-tap FIR filter can be defined as:

$$E_k(z) = e_{0k}z + e_{1k} + e_{2k}z^{-1}, \tag{15}$$

which corresponds to a non-causal form, though in practice, a causal implementation is employed for each equalizing structure. In order to obtain the values of each FIR filter of Eq. (15), some frequency points are selected at each k subchannel. Following the steps of [28–30], the frequency points $\omega = 0, \frac{\pi}{2}, \pi$, for even subbands, and $\omega = -\pi, -\frac{\pi}{2}, 0$, for odd subbands, are chosen. As a result, we get the following equations.

- Even subbands

$$E_k\left(e^{j\omega}\right) = \begin{cases} e_{0k} + e_{1k} + e_{2k} = \eta_{0k}, & \omega = 0, \\ je_{0k} + e_{1k} - je_{2k} = \eta_{1k}, & \omega = \dfrac{\pi}{2}, \\ -e_{0k} + e_{1k} - e_{2k} = \eta_{2k}, & \omega = \pi. \end{cases} \tag{16}$$

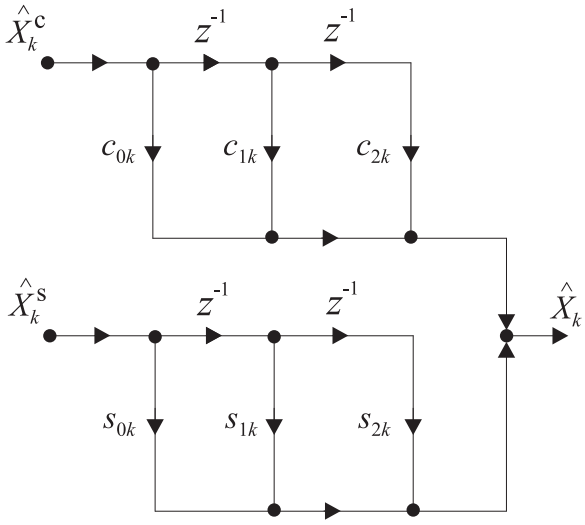

Fig. 4. Block diagram of each per-subcarrier equalizing structure of the 1-ASCET.

- Odd subbands

$$E_k\left(e^{j\omega}\right)=\begin{cases}-e_{0k}+e_{1k}-e_{2k}=\eta_{0k}, & \omega=-\pi,\\ -je_{0k}+e_{1k}+je_{2k}=\eta_{1k}, & \omega=-\dfrac{\pi}{2},\\ e_{0k}+e_{1k}+e_{2k}=\eta_{2k}, & \omega=0.\end{cases} \tag{17}$$

The subscript k denotes the subchannel under consideration, and

$$\eta_{ik}=\frac{H_{ch}^{*}\left(e^{j\frac{\pi}{4M}(2k+i)}\right)}{\left|H_{ch}\left(e^{j\frac{\pi}{4M}(2k+i)}\right)\right|^2+\dfrac{1}{SNR}}, \tag{18}$$

for $i=0,1,2$. We then obtain the coefficients for the 1-ASCET:

$$e_{0k}=\pm\frac{1}{2}\left(\frac{\eta_{0k}-\eta_{2k}}{2}-j\left(\eta_{1k}-\frac{\eta_{0k}+\eta_{2k}}{2}\right)\right), \tag{19a}$$

$$e_{1k}=\frac{\eta_{0k}+\eta_{2k}}{2}, \tag{19b}$$

$$e_{2k}=\pm\frac{1}{2}\left(\frac{\eta_{0k}-\eta_{2k}}{2}+j\left(\eta_{1k}-\frac{\eta_{0k}+\eta_{2k}}{2}\right)\right), \tag{19c}$$

where the positive signs stand for even subbands and the negative ones for odd subbands. Since e_{0k}, e_{1k} and e_{2k} are complex numbers, we have:

$$e_{ik}=c_{ik}-js_{ik},$$

where the real c_{ik} and the imaginary s_{ik} parts are, respectively, the filter coefficients of each equalizing structure of the 1-ASCET corresponding to the kth subband of the CM and SM filter bank, respectively (see Fig. 4).

5. Simulation results

In this section, we investigate the performance of a baseband system through computer simulations. In our first two experiments, we have considered several statistical in-home PLC model channels that synthesize different classes with a finite number of multipath components [31]. Specifically and in order to avoid the performance differences due to the severity of some channel's frequency response, the experiments consist in averaging the outcome of 100 transmissions through different impulse response realizations representative of Classes 1 (strong signal attenuation), 5 (medium attenuation) and 9 (little attenuation). The statistically representative channel frequency responses have been computed using the script available on-line in [32]. We have employed the release 2.0, that allows for the generation of channels according to the model parameters given in [31, Table I] for the different classes described in [33]. In the third experiment, we consider the model designed for broadband indoor power-line channel based on structural modeling of the power network presented in [34]. The impulse responses have been obtained using the software package *PLC_channel_generator_2*, available online in [35].

We have used the concatenated encoder proposed in [11], in which Reed–Solomon encoding is applied to the input data of the scrambler block, and then convolutional encoding is applied to

the output of the Reed–Solomon encoder. The coding rate of the encoder is 1/2, with constraint length 7, and generators 171 and 133 (octal). The third experiment also considers a different coding rate, 2/3, to evaluate its impact on the system performance. The output of the encoder is punctured following the recommended pattern [11].

For the simulations, the signal-to-noise ratio (SNR) is obtained from the receiver side, and several kinds of noise have been added to the receiving signals: Colored background noise (BGN), periodic impulsive noises synchronous and asynchronous (PINS and PINA), and a narrowband interference (NBI) with one frequency component located at 200 kHz, this one

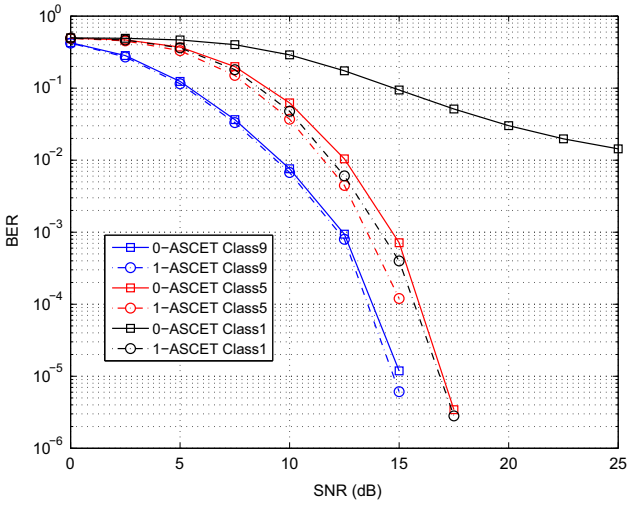

Fig. 5. BER performance comparison in 2-PAM under colored background, impulsive, synchronous and asynchronous noises.

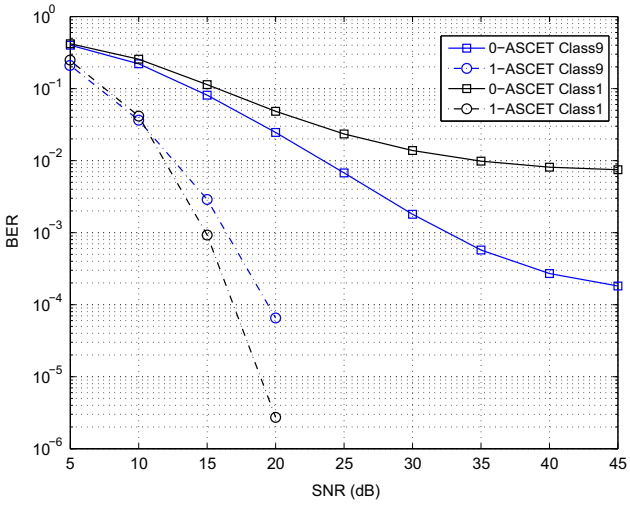

Fig. 6. BER performance comparison in 2-PAM under all different PLC noises.

simulating an interference from commercial AM radio station. All the above types of noise have been modeled following [36], where a detailed analysis of the indoor broadband power line noise components is presented.

For each SNR, more than one million binary data were generated and converted into parallel data to be transmitted over the active 360 subcarriers described in [11]. Before proceeding with the multicarrier modulation, the data at each subcarrier are mapped by 2-PAM. We assume that the channel remains unchanged within one symbol, though it changes independently among different symbols. Furthermore, we have also assumed both perfect synchronization and channel estimation. As receiver, we have employed the system of Fig. 3, with 0- and 1-ASCET.

The first set of experiments measures the BER performance of the transceiver system in the presence of BGN, PINS and PINA. Fig. 5 shows the average BER of the transceiver system considering classes 1, 5 and 9, each run over 100 different channels. The first remark that can be made on the results is that 1-ASCET always outperforms 0–ASCET. Nevertheless, and as it was expected, we can notice that the gains in the BER results for good channels (Class 9) are lower than the ones observed for the simulations of Classes 5 and 1. For instance, considering Class 9 channels, the 1-ASCET system shows gains of only 0.3 dB for BER $= 10^{-4}$, whereas for Class 5 is around 1 dB. Finally, the 1-ASCET for Class 1 exhibits BER values below 10^{-2} for SNR ≥ 11.9 dB, whereas more than 25 dB are needed to obtain a similar BER value with the 0-ASCET system.

As a second scenario, also NBI is considered in Classes 9 and 1. As can be seen in Fig. 6, the 1-ASCET shows a gain of around 16 dB for a BER value of 10^{-3} for Class 9. It even yields a better performance in Class 1: the BER value is below 10^{-4} for SNR ≥ 19.1 dB. Conversely, the systems reach error floors around 40 dB for 0–ASCET. In conclusion, the 1-ASCET outperforms the 0-ASCET scheme, but with different strength depending on the class of channels. The former really takes advantage over the latter for the most disturbed channels and under the presence of different types of noise.

In the last experiment, we compare the BER performance of the Wavelet OFDM transceiver in the presence of noise as described in the second scenario. In this experiment, we assume two representative LTI channels based on the physical structure of the electrical networks and labeled as best-case and worst-case (see [35]). For comparison, we consider as coding rates the values of

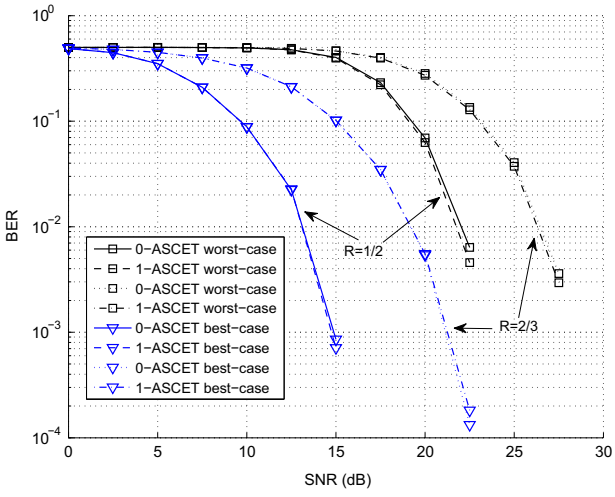

Fig. 7. BER performance comparison in 2-PAM under all different PLC noises and different coding rates.

1/2 and 2/3. As seen from Fig. 7, 1-ASCET does not achieve improvement performance compared to 0-ASCET. Furthermore and as expected, the best-case channel exhibits the best performance. Finally, increasing the value of the coding rate creates a separation in BER performance of around 6.5 dB (best-case) and 5 dB (worst-case) for $\mathrm{BER} = 5 \cdot 10^{-3}$.

6. Conclusion

This paper has presented some relevant aspects of the Wavelet OFDM physical layer for the baseband broadband communications over power line networks. The paper extends the understanding of the confusing terminology Wavelet OFDM, showing that the proposed scheme of modulation is a kind of cosine-modulated FBMC based on the extended lapped transform. The paper has also shown how to obtain the prototype filter coefficients recommended at the transmitter side. In addition, the focus was on the receiver side proposing an implementation based on polyphase filters. Further, we have investigated the performance of the frequency-domain equalizer system by means of computer experiments. Simulation results confirm that the proposed transceiver can be considered as an alternative approach to deal with low and high attenuation channels, considering different PLC scenarios.

Acknowledgments

The authors acknowledge the support provided by the Spanish Ministries of Economy and Competitiveness and Education, Culture, and Sport under Research Grants TEC2015-64835-C3-1-R, TEC2012-38058-C03-01 and PRX2014/00147.

The authors would like to thank the anonymous reviewers and the senior editor for their constructive suggestions which have helped in improving the paper.

References

[1] T. Hwang, C. Yang, G. Wu, S. Li, G. Li, OFDM and its wireless applications: a survey, IEEE Trans. Veh. Technol. 58 (4) (2009) 1673–1694, http://dx.doi.org/10.1109/TVT.2008.2004555.

[2] A. Sahin, İ. Güvenç, H. Arslan, A survey on multicarrier communications: prototype filters, lattice structures, and implementation aspects, IEEE Commun. Surv. Tutor. 16 (3) (2014) 1312–1338, http://dx.doi.org/10.1109/SURV.2013.121213.00263.

[3] P. Banelli, S. Buzzi, G. Colavolpe, A. Modenini, F. Rusek, A. Ugolini, Modulation formats and waveforms for 5G networks: who will be the heir of OFDM? IEEE Signal Process. Mag. (2014) 80–93.

[4] B. Farhang-Boroujeny, Filter bank multicarrier modulation: a waveform candidate for 5G and beyond, Adv. Electr. Eng. (2014).

[5] S. Premnath, D. Wasden, S.K. Kasera, N. Patwari, B. Farhang-Boroujeny, Beyond OFDM: best-effort dynamic spectrum access using filterbank multicarrier, IEEE/ACM Trans. Netw. 21 (3) (2013) 869–882, http://dx.doi.org/10.1109/TNET.2012.2213344.

[6] B. Farhang-Boroujeny, OFDM versus filter bank multicarrier, IEEE Signal Process. Mag. 28 (3) (2011) 92–112.

[7] H. Lin, P. Siohan, Capacity analysis for indoor PLC using different multi-carrier modulation schemes, IEEE Trans. Power Deliv. 25 (1) (2010) 113–124, http://dx.doi.org/10.1109/TPWRD.2009.2035277.

[8] P. Achaichia, M.L. Bot, P. Siohan, OFDM/OQAM: a solution to efficiently increase the capacity of future PLC networks, IEEE Trans. Power Deliv. 26 (4) (2011) 2443–2455, http://dx.doi.org/10.1109/TPWRD.2011.2140341.

[9] R. Ma, H.-H. Chen, Y.-R. Huang, W. Meng, Smart grid communication: its challenges and opportunities, IEEE Trans. Smart Grid 4 (1) (2013) 36–46, http://dx.doi.org/10.1109/TSG.2012.2225851.

[10] M.P. Tcheou, L. Lovisolo, M.V. Ribeiro, E.A.B. da Silva, M. Rodrigues, J.M.T. Romano, P.S.R. Diniz, The compression of electric signal waveforms for smart grids: state of the art and future trends, IEEE Trans. Smart Grid 5 (1) (2014) 291–302, http://dx.doi.org/10.1109/TSG.2013.2293957.

[11] IEEE Std 1901-2010, IEEE Standard for Broadband Over Power Line Networks: Medium Access Control and Physical Layer Specifications, 2010, pp. 1–1586, http://dx.doi.org/10.1109/IEEESTD.2010.5678772.

[12] M. Bellanger, J. Daguet, TDM-FDM transmultiplexer: digital polyphase and FFT, IEEE Trans. Commun. 22 (9) (1974) 1199–1205, http://dx.doi.org/10.1109/TCOM.1974.1092391.
[13] M. Bellanger, On computational complexity in digital transmultiplexer filters, IEEE Trans. Commun. 30 (7) (1982) 1461–1465, http://dx.doi.org/10.1109/TCOM.1982.1095651.
[14] B. Farhang-Boroujeny, C.H. Yuen, Cosine modulated and offset QAM filter bank multicarrier techniques: a continuous-time prospect, EURASIP J. Adv. Signal Process. 2010 (2010) 6.
[15] S.A. Elghafar, S.M. Diab, B.M. Sallam, E.S. Hassan, M. Shokair, W. Al-Nauimy, M.I. Dessouky, E.M. El-Rabaie, S. Alshebeili, F.E.A. El-Samie, Utilization of discrete transforms to conquer the problems of multi-tone systems, J. Frankl. Inst. 351 (3) (2014) 1778–1800.
[16] R.E. Crochiere, L.R. Rabiner, Multirate Digital Signal Processing, Prentice Hall, Englewood Cliffs, New Jersey, 1983.
[17] F. Cruz-Roldán, M. Blanco-Velasco, Joint use of DFT filter banks and modulated transmultiplexers for multicarrier communications, Signal Process. 91 (7) (2011) 1622–1635, http://dx.doi.org/10.1016/j.sigpro.2011.01.006.
[18] F. Cruz-Roldán, M. Blanco-Velasco, J.I.G. Llorente, Zero-padding or cyclic prefix for MDFT-based filter bank multicarrier communications, Signal Process. 92 (7) (2012) 1646–1657, http://dx.doi.org/10.1016/j.sigpro.2011.12.023.
[19] H. Malvar, Signal Processing with Lapped Transforms, Artech House, Norwood, MA, 1992.
[20] R.D. Koilpillai, P.P. Vaidyanathan, Cosine-modulated FIR filter banks satisfying perfect reconstruction, IEEE Trans. Signal Process. 40 (4) (1992) 770–783.
[21] S.A. Martucci, Symmetric convolution and the discrete sine and cosine transform, IEEE Trans. Signal Process. 42 (5) (1994) 1038–1051.
[22] V. Sánchez, P. García, A.M. Peinado, J.C. Segura, A.J. Rubio, Diagonalizing properties of the discrete cosine transform, IEEE Trans. Signal Process. 43 (11) (1995) 2631–2641.
[23] P. Vaidyanathan, Passive cascaded-lattice structures for low-sensitivity FIR filter design, with applications to filter banks, IEEE Trans. Circuits Syst. 33 (11) (1986) 1045–1064, http://dx.doi.org/10.1109/TCS.1986.1085867.
[24] V. Britanak, The fast DCT-IV/DST-IV computation via the MDCT, Signal Process. 83 (8) (2003) 1803–1813.
[25] G. Plonka, M. Tasche, Fast and numerically stable algorithms for discrete cosine transforms, Linear Algebra. Appl. 394 (1) (2005) 309–345.
[26] X. Shao, A.G. Johnson, Type-IV DCT, DST, and MDCT algorithms with reduced numbers of arithmetic operations, Signal Process. 88 (6) (2008) 1313–1326.
[27] J. Alhava, M. Renfors, Adaptive sine-modulated/cosine-modulated filter bank equalizer for transmultiplexers, In: European Conference on Circuit Theory and Design, Espoo, Finland, 2001, pp. 337–340.
[28] K. Izumi, D. Umehara, S. Denno, Performance evaluation of wavelet OFDM using ASCET, In: IEEE International Symposium on Power Line Communications and its Applications, 2007, ISPLC'07, 2007, pp. 246–251. http://dx.doi.org/10.1109/ISPLC.2007.371131.
[29] Y. Yang, T. Ihalainen, M. Rinne, M. Renfors, Frequency-domain equalization in single-carrier transmission: filter bank approach, EURASIP J. Appl. Signal Process. 2007 (1) (2007) 135.
[30] T. Ihalainen, T. Hidalgo Stitz, M. Rinne, M. Renfors, Channel equalization in filter bank based multicarrier modulation for wireless communications, EURASIP J. Adv. Signal Process. (2007), 10.1155/2007/49389.
[31] A. Tonello, S. D'Alessandro, L. Lampe, Cyclic prefix design and allocation in bit-loaded OFDM over power line communication channels, IEEE Trans. Commun. 58 (11) (2010) 3265–3276, http://dx.doi.org/10.1109/TCOMM.2010.092810.090447.
[32] A. Tonello, Brief Tutorial on the Statistical Top-Down PLC Channel Generator ⟨http://www.diegm.uniud.it/tonello/plcresearch.html⟩, 2010.
[33] Seventh Framework Programme: Theme 3 ICT-213311 OMEGA, PLC Channel and Modelling, Technical Report ⟨http://www.ict-omega.eu/ ⟩, 2008.
[34] F.J. Cañete, J.A. Cortés, L. Díez, J.T. Entrambasaguas, A channel model proposal for indoor power line communications, IEEE Commun. Mag. 49 (12) (2011) 166–174, http://dx.doi.org/10.1109/MCOM.2011.6094022.
[35] F.J. Cañete, User Guide for PLC Channel Generator v.2 ⟨http://www.plc.uma.es/canales.htm⟩, 2011.
[36] J.A. Cortés, L. Díez, F.J. Cañete, J.J. Sánchez-Martínez, Analysis of the indoor broadband power-line noise scenario, IEEE Trans. Electromagn. Compat. 52 (4) (2010) 849–858, http://dx.doi.org/10.1109/TEMC.2010.2052463.